IVYSPRING INTERNATIONAL PUBLISHER

International Journal of Medical Sciences

2026; 23(12): 3754-3767. doi: 10.7150/ijms.132718

Research Paper

Glucosamine Attenuates the Hydroquinone-induced Cell Damage in ARPE-19 cells via ROS-OGT-SIRT1 Pathway

Hsin-Ting Lin[1,2], Jiann-Torng Chen[1,2], Yi-Hao Chen[1,2], Chu-Yen Chien[3], Cai-Mei Zheng[4,5,6,7], Ching-Long Chen[1,2]✉

1. Department of Ophthalmology, Tri-Service General Hospital, National Defense Medical University, Taipei 114, Taiwan.
2. Graduate Institute of Medical Sciences, College of Medicine, National Defense Medical University, Taipei 114, Taiwan.
3. School of Dentistry, National Defense Medical University, Taipei 114, Taiwan.
4. Division of Nephrology, Department of Internal Medicine, School of Medicine, College of Medicine, Taipei Medical University, Taipei 110, Taiwan.
5. TMU Research Center of Urology and Kidney, Taipei Medical University, Taipei 110, Taiwan.
6. Division of Nephrology, Department of Internal Medicine, Shuang Ho Hospital, Taipei Medical University, Taipei 235, Taiwan.
7. Graduate Institute of Clinical Medicine, College of Medicine, Taipei Medical University, Taipei 110, Taiwan.

✉ Corresponding author: **Ching-Long Chen, MD, PhD.,** Ching-Long Chen, Department of Ophthalmology, Tri-Service General Hospital, National Defense Medical University, Taipei 114, Taiwan. Email: doc30881@mail.ndmutsgh.edu.tw; Phone: 886-2-87923311.

© The author(s). This is an open access article distributed under the terms of the Creative Commons Attribution License (https://creativecommons.org/licenses/by/4.0/). See https://ivyspring.com/terms for full terms and conditions.

Received: 2026.02.05; Accepted: 2026.10.23; Published: 2026.11.13

Abstract

Age-related macular degeneration (AMD) is a leading cause of vision loss, with oxidative stress playing a central role in its pathogenesis. Hydroquinone (HQ), a major pro-oxidant in cigarette smoke, contributes to retinal pigment epithelial (RPE) cell degeneration. Although glucosamine (GlcN) has shown protective effects against AMD, the underlying mechanisms remain poorly understood. Human RPE cells were treated with HQ to induce oxidative stress and cellular injury. Reactive oxygen species (ROS) levels and glutathione content were measured to assess oxidative stress and antioxidant capacity. Cellular damage was evaluated using CCK-8 and LDH assays. The role of SIRT1 was investigated through RNA interference and overexpression studies. SIRT1 O-GlcNAcylation was assessed by co-immunoprecipitation and Western blot, and protein stability was examined using a cycloheximide-chase assay. Our results showed HQ exposure impaired antioxidant defenses and induced apoptosis by downregulating SIRT1 in ARPE-19 cells. Mechanistically, HQ enhanced the interaction between SIRT1 and O-GlcNAc transferase (OGT), promoting SIRT1 O-GlcNAcylation and degradation. GlcN treatment restored glutathione levels, reduced apoptosis, and reversed both morphological and molecular damage by stabilizing SIRT1 expression. Notably, the protective effects of GlcN were diminished upon SIRT1 silencing, confirming the central role of SIRT1 in mediating its effects. Our study indicated GlcN protects against HQ-induced RPE degeneration by reducing ROS, thus decreasing SIRT1 glycosylation and enhancing its stability. These findings identify the ROS-OGT-SIRT1 axis as an important regulatory signaling in HQ-induced RPE cellular dysfunction and support that GlcN represents a cytoprotective agent for preserving RPE homeostasis under oxidative stress.

Keywords: age-related macular degeneration, hydroquinone, glucosamine, SIRT1, glycosylation

Introduction

Age-related macular degeneration (AMD) is one of the leading causes of visual impairment and severe vision loss worldwide [1]. Currently, it is estimated that approximately 200 million people are affected by AMD globally [2]. AMD is a progressive disease of the central retina that can be stabilized but not fully cured [1]. The retinal pigment epithelial (RPE) maintains the retinal microenvironment through selective transport and phagocytosis of photoreceptor outer segments. Dysfunction or loss of RPE cells is a hallmark of late-stage dry AMD and may also contribute to wet AMD [3]. Due to their high oxygen demand and continuous exposure to light, RPE cells rely on strong intrinsic antioxidant defenses [4]. However, these protective

mechanisms are compromised in AMD patients [5].

Major risk factors for AMD include age, smoking, and low dietary intake of antioxidants [6]. Among these, smoking is the most significant modifiable risk factor. It has been associated with a two-fold increase in the risk of developing late-stage AMD and with an earlier onset [7, 8]. Current smokers are more likely to develop AMD at a younger age compared to never-smokers or former smokers who quit over 10 years ago [9]. Smoking induces oxidative stress, lipid peroxidation, elevated fibrinogen levels, increased platelet aggregation, and decreased levels of plasma high-density lipoprotein and antioxidants [10, 11]. *In vitro* studies have revealed smoking caused decreases of intracellular GSH, cell size, and nuclear condensation and increases of lipid peroxidation and mitochondrial superoxide in human RPE cells [12]. Consistently, *in vivo* studies have showed that smoking induced oxidative stress and apoptosis in RPE cells [13, 14]. Hydroquinone (HQ), a prominent component of cigarette smoke, has been widely used in mouse models to induce RPE dysfunction and the formation of sub-RPE deposits [14, 15]. *In vitro* studies have shown that HQ induces dose-dependent cell death, reduces mitochondrial membrane potential, and triggers autophagy, inflammation, endoplasmic reticulum (ER) stress and the unfolded protein response (UPR) in RPE cells [16-19]. However, the underlying mechanisms involved in HQ-induced RPE dysfunction are still under investigation.

Sirtuin 1 (SIRT1), a member of the sirtuin family encoded by the *SIRT1* gene, functions as a nicotinamide adenine dinucleotide (NAD+)-dependent deacetylase, targeting lysine residues of both histone and non-histone proteins [20]. SIRT1 has been shown to regulate cell proliferation, oxidative stress responses, apoptosis, and inflammation in various disease models [21]. Moreover, SIRT1 protein levels have been reported to be significantly reduced in RPE derived from human AMD donor eyes compared with normal donor RPE, and that it has been implicated in protecting retinal cells by modulating oxidative and inflammatory pathways [22]. Notably, HQ has been noted to modulate SIRT1 expression in lymphoblastoid cells [23]. However, the effect of HQ on the expression of SIRT1 in RPE cells is less understood.

Glucosamine (GlcN), a naturally occurring amino monosaccharide, has been widely used as a dietary supplement with a favorable safety profile for long-term human use [24]. A retrospective, population-based cohort study reported a lower risk of developing dry AMD among GlcN users compared to non-users [25]. It has been extensively studied both *in vitro* and *in vivo* for its anti-apoptotic and anti-inflammatory effects to protect RPE cells [26-28]. Mechanistically, GlcN has been observed to activate autophagy through AMPK-mTOR pathway, leading to reduced lipofuscin accumulation in ARPE-19 cells [29]. In addition, GlcN has been shown to upregulate expression of SIRT1 in human chondrocyte cells [30]. However, the mechanisms by which GlcN influences AMD progression remain unclear.

In this study, we aimed to investigate the role of SIRT1 in HQ-induced RPE cell dysfunction and to evaluate the potential protective effects of GlcN. Specifically, we explored whether GlcN modulates SIRT1 expression and mitigates oxidative stress and apoptosis in RPE cells exposed to HQ, thereby elucidating molecular pathways relevant to RPE survival under oxidative challenge.

Materials and Methods

Cell line and cell culture

ARPE-19 cells were obtained from the American Type Culture Collection (ATCC, Manassas, VA, USA) and cultured in DMEM/F-12 medium (GIBCO, Eggenstein, Germany) supplemented with 10% fetal bovine serum (FBS; GIBCO, Eggenstein, Germany) and 1% Penicillin-Streptomycin-Amphotericin B (PSA; Biological Industries, Cromwell, CT, USA). Primary human retinal pigment epithelial (hRPE) cells and epithelial cell medium (EpiCM) were purchased from ScienCell Research Laboratories (San Diego, CA, USA) and the cells were cultured according to the manufacturer's instructions.

Drugs and antibodies

HQ and GlcN were purchased from Sigma-Aldrich (St. Louis, MO, USA) and dissolved in sterile distilled water. N-acetyl cysteine (NAC; Sigma-Aldrich) was used as a ROS inhibitor and prepared in dimethyl sulfoxide (DMSO; Sigma-Aldrich). Primary antibodies were obtained from Cell Signaling Technology (Beverly, MA, USA). Horseradish peroxidase (HRP)-conjugated secondary antibodies were purchased from Jackson ImmunoResearch (West Grove, PA, USA).

RNA sequencing analysis

High-throughput mRNA sequencing was performed on a NovaSeq 6000 platform (Illumina, San Diego, CA, USA). Sequencing data (FASTQ files) were processed, aligned, and analyzed using the CLC Genomics Workbench software, version 21 (Qiagen, Hilden, Germany). Differentially expressed genes (DEGs) were identified using a threshold of $|\log_2(\text{Fold Change})| > 1.2$ and a p-value < 0.05. Heat maps were generated using the Morpheus online tool.

RNA interference, plasmids, and transfection

Non-targeting scrambled small interfering RNA (siRNA) and SIRT1-targeting siRNA were synthesized by Dharmacon (Lafayette, CO, USA). The siRNA sequences were as follows: scrambled control, 5′-UAGCGACUAAACACAUCAA-3′; SIRT1 siRNA, 5′-GGAUAGGUCCAUAUACUUU-3′. For gene silencing, ARPE-19 cells were seeded in 6-well plates and transfected with 25 nM siRNA using GenMute transfection reagent (SignaGen Laboratories, Ijamsville, MD, USA). For overexpression experiments, cells were transfected with 1 μg of *SIRT1*-overexpressing plasmids using PolyJet transfection reagent (SignaGen Laboratories) following the manufacturer's protocol.

Cell viability assay

Cell viability was assessed using a cell counting kit-8 reagent (CCK-8; Abbkine, Atlanta, GA, USA). ARPE-19 cells were seeded in 96-well plates and incubated overnight. After treatments, 10 μl of CCK-8 reagent was added to each well and incubated at 37 °C for 1 hour. Absorbance was measured at 450 nm using a microplate reader.

Cell cytotoxicity assay

Cellular cytotoxicity was evaluated using a Lactate Dehydrogenase (LDH) assay kit (Cayman Chemical, Ann Arbor, MI, USA). Conditioned medium was collected and incubated with LDH reaction reagent at 37 °C for 30 minutes. Absorbance was recorded at 490 nm using a microplate reader.

Caspase-3 activity assay

Caspase-3 activity was measured using a QuantiFluo Caspase-3 Assay Kit (BioAssay Systems, Hayward, CA, USA). ARPE-19 cells were seeded in 96-well plates (2×10^4 cells/well) and incubated overnight. After treatment, N-Ac-DEVD-AFC substrate was added and incubated at 37 °C for 1 hour. The substrate was cleaved by active caspase-3 of apoptotic cells, thus generating a highly fluorescent product. Fluorescence intensity was measured at an excitation/emission of 400/490 nm using a fluorescence plate reader.

Annexin V-DRAQ7 double staining assay

Apoptosis was assessed using Annexin V-FITC/Deep Red Anthraquinone 7 (DRAQ7) staining (Elabscience, Houston, TX, USA) followed by flow cytometry. Treated cells were harvested, washed with PBS, and resuspended in binding buffer containing Annexin V-FITC and DRAQ7. Apoptotic cells were analyzed using a FACSCalibur flow cytometer (BD Biosciences, San Jose, CA, USA), and data were processed using CellQuest Pro software (BD Biosciences, San Jose, CA, USA).

ROS detection assay

Intracellular ROS levels were detected using a ROS Detection Kit (Cayman Chemical Company, Ann Arbor, MI, USA). The cells were seeded at 2×10^4 cells in 96-well culture plates, incubated overnight, and treated as indicated. Cells were stained with 2′,7′-dichlorodihydrofluorescein diacetate (DCFDA) at 37 °C for 30 minutes. Pyocyanin and NAC were used as positive and negative controls, respectively. Fluorescence was measured at 485/520 nm (excitation/emission) using a fluorescence microplate reader.

Glutathione detection assay

Intracellular reduced glutathione (GSH) levels were quantified using the QuantiChrom Glutathione assay kit (BioAssay Systems, Hayward, CA, USA). Cell lysates from 2×10^6 cells were mixed with 5,5′-dithiobis-(2-nitrobenzoic acid) (DTNB), which reacts with GSH to form the yellow-colored product, 5-thio-2-nitrobenzoic acid (TNB). Absorbance was measured at 412 nm using a microplate reader.

Cycloheximide (CHX) Chase Assay

The stability and degradation of SIRT1 protein were analyzed using a CHX chase assay. CHX (50 μg/mL) functioned as a translation elongation inhibitor and used to restrict protein translation. Cells were collected at 0, 6, 18, and 30 hours post-treatment, and SIRT1 levels were assessed by Western blot.

Co-immunoprecipitation (Co-IP) and western blot analysis

Total cell lysates were prepared using RIPA buffer supplemented with protease and phosphatase inhibitors (Biological industries, Cromwell, CT, USA). Co-IP was performed to examine the O-linked glycosylation of SIRT1 and interaction between SIRT1 and O-GlcNAc transferase (OGT). Equal amounts of protein lysates were incubated overnight at 4 °C with anti-SIRT1 antibodies and then pulled down using protein G Sepharose beads (GE Healthcare, Piscataway, NJ, USA) for 4 hours at 4 °C. Precipitated proteins were denatured with sample buffer and heated at 100 °C. The expressions of respective proteins were analyzed using Western blot analysis. Total proteins were resolved by sodium dodecyl sulfate-polyacrylamide gel electrophoresis (SDS-PAGE), transferred to PVDF membranes, blocked in 5% non-fat milk in 0.1% TBS-T, and incubated with primary antibodies overnight at 4 °C. Membranes were washed and probed with HRP-conjugated

secondary antibodies, and signals were visualized using ECL reagents (Merck Millipore, Darmstadt, Germany). Images were obtained using a chemiluminescence image system (UVP Inc., San Gabriel, CA, USA), and band intensity was quantified using ImageJ software.

SIRT1 activity assay

SIRT1 enzymatic activity was analyzed using a SIRT1 activity assay kit (Abcam, Cambridge, UK) according to the manufacturer's instructions. Cell lysates were incubated with the provided enzymatic reaction buffer, and SIRT1-mediated deacetylation was quantified by measuring fluorescence intensity. Signals were detected using a fluorescence microplate reader with excitation and emission wavelengths at 350 nm and 450 nm, respectively.

Immunofluorescence staining

Cellular co-localization of SIRT1 and OGT was assessed via immunofluorescence (IF) staining. ARPE-19 cells were fixed with 4% paraformaldehyde, permeabilized with 0.1% Triton X-100, and blocked in 5% bovine serum albumin (BSA). Cells were incubated overnight at 4 °C with primary antibodies against SIRT1 and OGT, followed by incubation with Alexa Fluor 555- and Alexa Fluor 488-conjugated secondary antibodies (Invitrogen, Carlsbad, CA, USA), respectively. Fluorescent images were acquired using a Leica DMi8 THUNDER Imager with 100x oil-immersion objectives. The spatial interaction between SIRT1 and OGT was quantified by Pearson's correlation coefficient using the Coloc2 plugin in ImageJ/Fiji. Quantitative measurements were derived from five random fields per treatment group in each of three independent experiments.

Statistical analysis

Data are presented as mean ± SEM. Statistical analysis and graphical representations were performed using GraphPad Prism software (version 5.01; GraphPad Software Inc., San Diego, CA, USA). One-way ANOVA followed by Bonferroni's post hoc test was used for comparisons among multiple groups. The CHX chase assay was analyzed using two-way ANOVA. A p value less than 0.05 was considered statistically significant (*$p < 0.05$, **$p < 0.01$, ***$p < 0.001$).

Results

HQ caused dose-dependent increased in morphological alteration, oxidative stress, and cellular damage in ARPE-19 cells

To investigate the pathological impact of HQ on RPE function, ARPE-19 cells were exposed to increasing concentrations of HQ (62.5-500 μM). Morphological analysis revealed that untreated cells displayed a cobblestone-like morphology. Treatment with 250 and 500 μM of HQ resulted in a more rounded and shrunken appearance in ARPE-19 cells (Figure 1A). ROS production significantly increased in cells treated with 125 and 250 μM HQ but decreased at 500 μM (Figure 1B). Furthermore, antioxidant capacity, indicated by intracellular glutathione levels (Figure 1C), and cell viability (Figure 1D) were markedly reduced following HQ exposure. HQ also induced cytotoxicity (Figure 1E) and activated the pro-apoptotic enzyme caspase-3 (Figure 1F). Flow cytometry confirmed a substantial increase in apoptotic cells following HQ treatment (Figure 1G). Of note, ROS levels decreased at 500 μM of HQ (Figure 1B), which was likely attributable to severe cytotoxicity and loss of viable cells rather than a biological reduction in oxidative stress, as supported by the marked increase in LDH release at this concentration (Figure 1E). As the most pronounced pathological effects occurred at 250 μM HQ, this concentration was used in subsequent experiments. To investigate changes in gene expression, RNA sequencing (RNA-seq) followed by Ingenuity Pathway Analysis (IPA) was conducted in ARPE-19 cells treated with or without 250 μM HQ (Figure 1H). DEGs were defined as $|\log_2(\text{Fold Change})| > 1.2$ and a p value less than 0.05. HQ exposure upregulated genes related to inflammation (*RELA, RELB, NFKB2, VEGFA*), apoptosis (*BNIP3, PIDD1, IRAK2, CASP3, BAX*), and oxidative stress (*HMOX1, NCF2, RAC2, FOS, JUN, ANGPTL4*), while downregulating genes involved in anti-inflammation (*CHUK, MTURN*), anti-apoptosis (*CFLAR, BCL2, XIAP*), and antioxidant defense (*CREB1, NRROS, GPX8, MAF, EPHX2*). Although neither *SIRT1* nor *SOX9* met the predefined criterion for classification as a DEG, their transcript levels were further examined because of their specific relevance to the present study. RNA-seq analysis showed that *SOX9* mRNA was significantly decreased following HQ exposure ($\log_2FC = -0.462$, $p < 0.001$), whereas SIRT1 transcript levels remained unchanged ($\log_2FC = 0.017$, $p = 0.927$) (Table S1). These results indicated that HQ exacerbated RPE degeneration by promoting oxidative stress, apoptosis, and inflammation in ARPE-19 cells, and that protein level of SIRT1 may be regulated independent of its transcription in HQ-exposed cells.

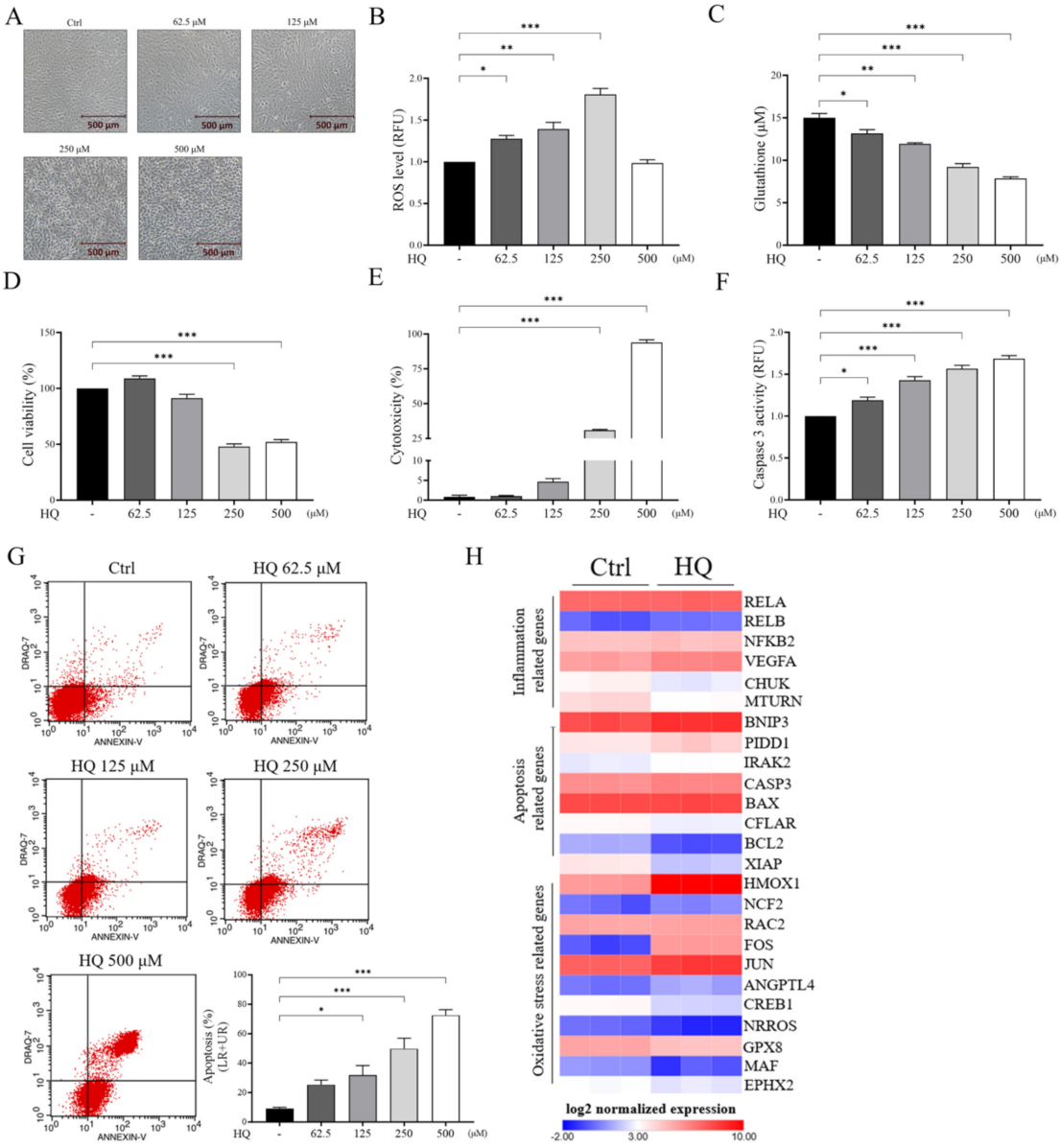


Figure 1. Hydroquinone induced oxidative stress and cytotoxicity in ARPE-19 cells in a dose-dependent manner. ARPE-19 cells were treated with various doses (0, 62.5, 125, 250, and 500 μM) of HQ. (A) The morphological changes of HQ-exposed cells were observed and captured using a microscopy equipped with a camera. (B) The reactive oxidative stress (ROS) production was measured using a ROS detection cell-based assay kit. (C) The intracellular glutathione (GSH) contents were detected using a GSH assay kit. (D) The viability of cells was determined using a cell counting kit-8 (CCK-8) reagent. (E) The cell damage was examined using a lactate dehydrogenase (LDH) assay kit. (F) The caspase-3 activity was investigated using a caspase-3 assay kit. (G) The apoptosis of ARPE-19 cells after indicated treatments were evaluated using Annexin V-FITC and DRAQ7 double staining followed by flow cytometry. Representative images are shown (left panels). The bar chart shows the quantitative results of cell apoptosis (right panel). (H) The heat map illustrates RNA-seq differential expression results of genes involved in inflammation, apoptosis, and oxidative stress in ARPE19 cells with/without HQ exposure. Red and blue colors represent highly- and lowly-expressed genes, respectively. HQ, hydroquinone. LR, lower right. UR, upper right. *p < 0.05, **p < 0.01, ***p < 0.001 by one-way ANOVA followed by Bonferroni's post hoc test. Data are presented as the mean ± SEM. SEM, error bars. Scale bar, 500 μm.

Oxidative stress functioned as an upstream regulator in HQ-mediated SIRT1 downregulation and RPE dysfunction in ARPE-19 cells

To investigate the role of HQ-induced oxidative stress in AMD pathology of ARPE-19 cells, we employed NAC, a known antioxidant and ROS scavenger [31]. NAC suppressed HQ-induced ROS generation (Figure 2A), disruption of antioxidant machinery (Figure 2B), and morphological alterations (Figure 2C). In addition, it significantly improved cell viability (Figure 2D), decreased LDH release (Figure 2E), and reduced caspase-3 activation (Figure 2F) and apoptosis (Figure 2G) in HQ-exposed cells. NAC treatment reversed HQ-induced changes in PCNA and NRF2 expressions. It also reduced cleaved caspase-3 level and further increased HO-1 expression (Figure 2H). Given that protective roles of SIRT1 and its downstream effector have been noted in AMD development [32], and transcriptomic profiling revealed that while the downstream target SOX9 was significantly downregulated by HQ exposure, SIRT1

mRNA levels remained unaltered (Supplementary Table S1). This apparent divergence between stable SIRT1 transcription and suppressed downstream target expression suggested that HQ impaired SIRT1 through affecting protein abundance or enzymatic activity rather than through transcriptional repression. Consequently, we next evaluated whether HQ exposure affected SIRT1 at the protein level. As shown in Figure 2H, HQ suppressed the expressions of SIRT1 and SOX9, and that these effects were reversed by NAC in ARPE-19 cells. These results indicated HQ induced AMD-associated changes and SIRT1 downregulation in ARPE-19 cells through ROS induction.

HQ induced functional dysregulation of ARPE-19 cells through the downregulation of SIRT1

To investigate whether the decreased expression of SIRT1 contributed to HQ-induced AMD pathology, ARPE-19 cells were transfected with SIRT1-overexpressing plasmids or empty vectors (EV) followed by exposure to 250 μM HQ. We observed the mRNA and protein levels of SIRT1 were markedly increased in cells transfected with SIRT1 overexpressing plasmids (Figure 3A). Although HQ did not affect *SIRT1* mRNA levels (Figure 3B), it markedly reduced protein expressions of SIRT1 and SOX9 (Figure 3C). Notably, SIRT1 activity was also rescued in SIRT1-overexpressing cells in response to HQ treatment (Figure S1). HQ exposure decreased

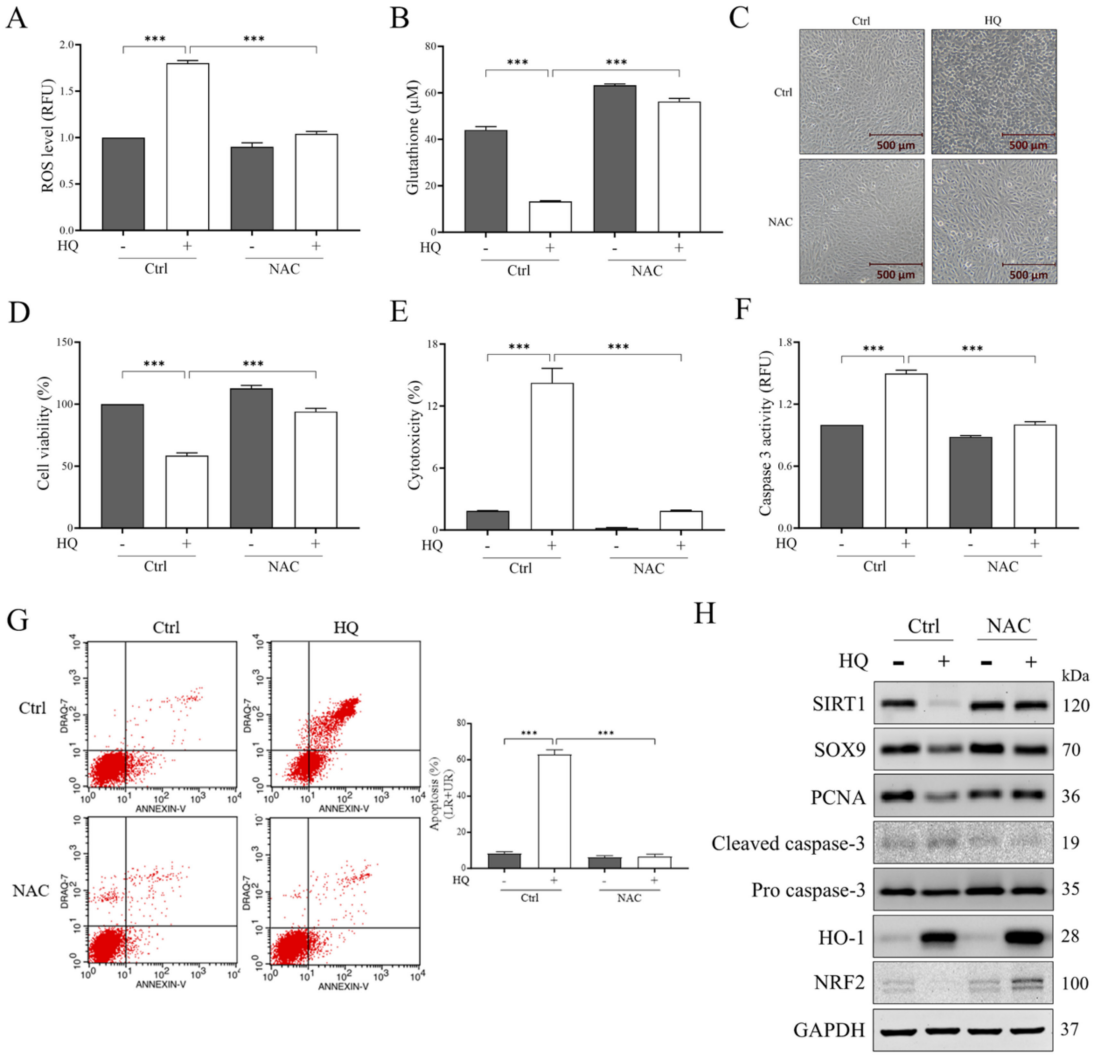


Figure 2. N-acetylcysteine ameliorated hydroquinone-triggered oxidative stress, apoptosis, and SIRT1 downregulation in ARPE-19 cells. ARPE-19 cells were pre-treated with/without 5 mM of NAC followed by exposure to 250 μM of HQ for 6 hours. (A) The reactive oxidative stress (ROS) levels were measured using a ROS detection cell-based assay kit. (B) A GSH assay kit was applied to detect intracellular amounts of glutathione (GSH). (C) Representative images show the morphological changes of ARPE-19 cells after indicated treatments. (D) The cell viability was determined using a cell counting kit-8 (CCK-8) reagent. (E) The cytotoxicity was investigated using a lactate dehydrogenase (LDH) assay kit. (F) The activity of caspase-3 was analyzed using a caspase-3 assay kit. (G) Annexin V-FITC and DRAQ7 double staining of apoptotic cells was measured using flow cytometry. Representative images are shown (left panels). The bar chart shows the quantitative results of apoptotic cells (right panel). (H) The expressions of markers of DNA repair (PCNA), oxidative stress (HO-1 and NRF2), apoptosis (cleaved caspase-3 and pro caspase-3), SIRT1, and SOX9, in ARPE-19 cells were analyzed using Western blot analysis. HQ, hydroquinone. NAC, N-acetylcysteine. LR, lower right. UR, upper right. GAPDH was used as the loading control. ***p < 0.001 by one-way ANOVA followed by Bonferroni's post hoc test. Data are presented as the mean ± SEM. SEM, error bars. Scale bar, 500 μm.

PCNA and NRF2 levels and increased cleaved caspase-3 and HO-1 expressions (Figure 3C). Overexpression of SIRT1 reversed these effects, except that it further enhanced HO-1 expression in HQ-treated cells (Figure 3C). SIRT1 overexpression ameliorated HQ-induced morphological changes (Figure 3D), restored intracellular glutathione levels (Figure 3F), and mitigated HQ-induced cell damage (Figures 3G and 3H) and apoptosis (Figures 3I and 3J), but it did not reduce ROS production (Figure 3E). These findings demonstrated that while SIRT1 did not directly quench HQ-induced ROS, its overexpression effectively mitigated downstream cellular consequences, including morphological deterioration, glutathione depletion, and cell apoptosis in cells after exposure to HQ.

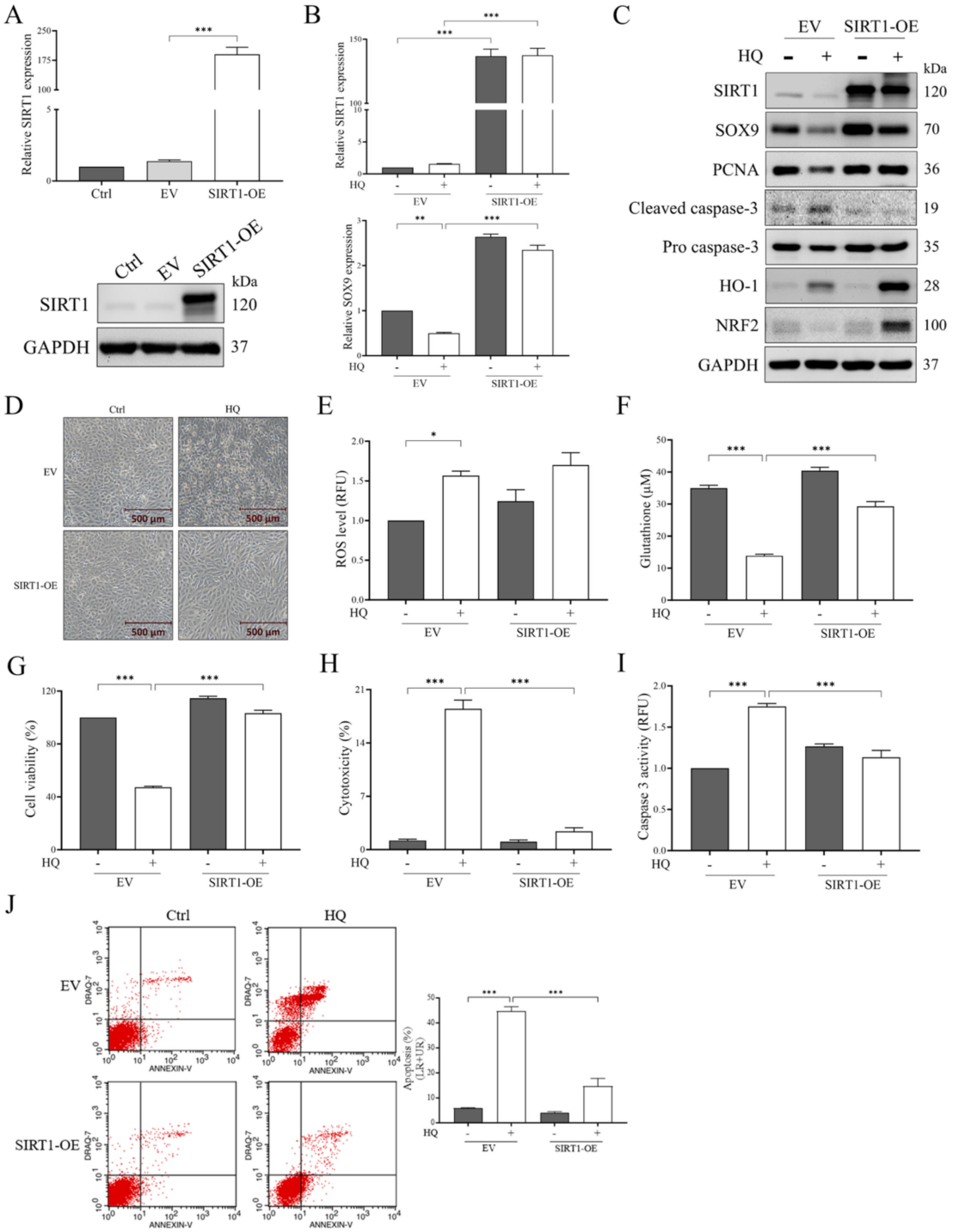


Figure 3. Ectopic SIRT1 expression provided cytoprotection against hydroquinone-induced morphological dysregulation, reduction in glutathione, and cell injury independently of reactive oxygen species-scavenging activity in ARPE-19 cells. ARPE-19 cells were transfected with either empty vector or SIRT1-overexpressing plasmids followed by exposure to 250 μM of HQ for 6 hours. (A) The expression of SIRT1 was examined using quantitative RT-PCR (upper panel) and Western blot analysis (lower panel). (B and C) mRNA and protein expressions of SIRT1, SOX9, and markers of DNA repair (PCNA), apoptosis (cleaved caspase-3 and pro caspase-3),

and oxidative stress (HO-1 and NRF2) in ARPE-19 cells after indicated treatments were analyzed using quantitative RT-PCR (B) or Western blot analysis (C). (D) The morphological alterations were captured using a microscopy equipped with a camera. (E) Generation of reactive oxidative stress (ROS) was detected using a ROS detection cell-based assay kit. (F) Intracellular amounts of glutathione (GSH) were investigated using a GSH assay kit. (G) The cells survival was determined using a cell counting kit-8 (CCK-8) reagent. (H) The cell cytotoxicity was evaluated using a lactate dehydrogenase (LDH) assay kit. (I) The caspase-3 activity was observed using a caspase-3 assay kit. (J) After respective treatments, Annexin V-FITC and DRAQ7-stained apoptotic cells were quantified using flow cytometry. Representative images are shown in left panels. Quantitative results of apoptotic cells are shown in right panel. HQ, hydroquinone. EV, empty vector plasmids-transfected cells. SIRT1-OE, SIRT1-overexpressing plasmids-transfected cells. LR, lower right. UR, upper right. GAPDH served as the loading control. *p < 0.05, **p < 0.01, ***p < 0.001 by one-way ANOVA followed by Bonferroni's post hoc test. Data are expressed as the mean ± SEM. SEM, error bars. Scale bar, 500 μm.

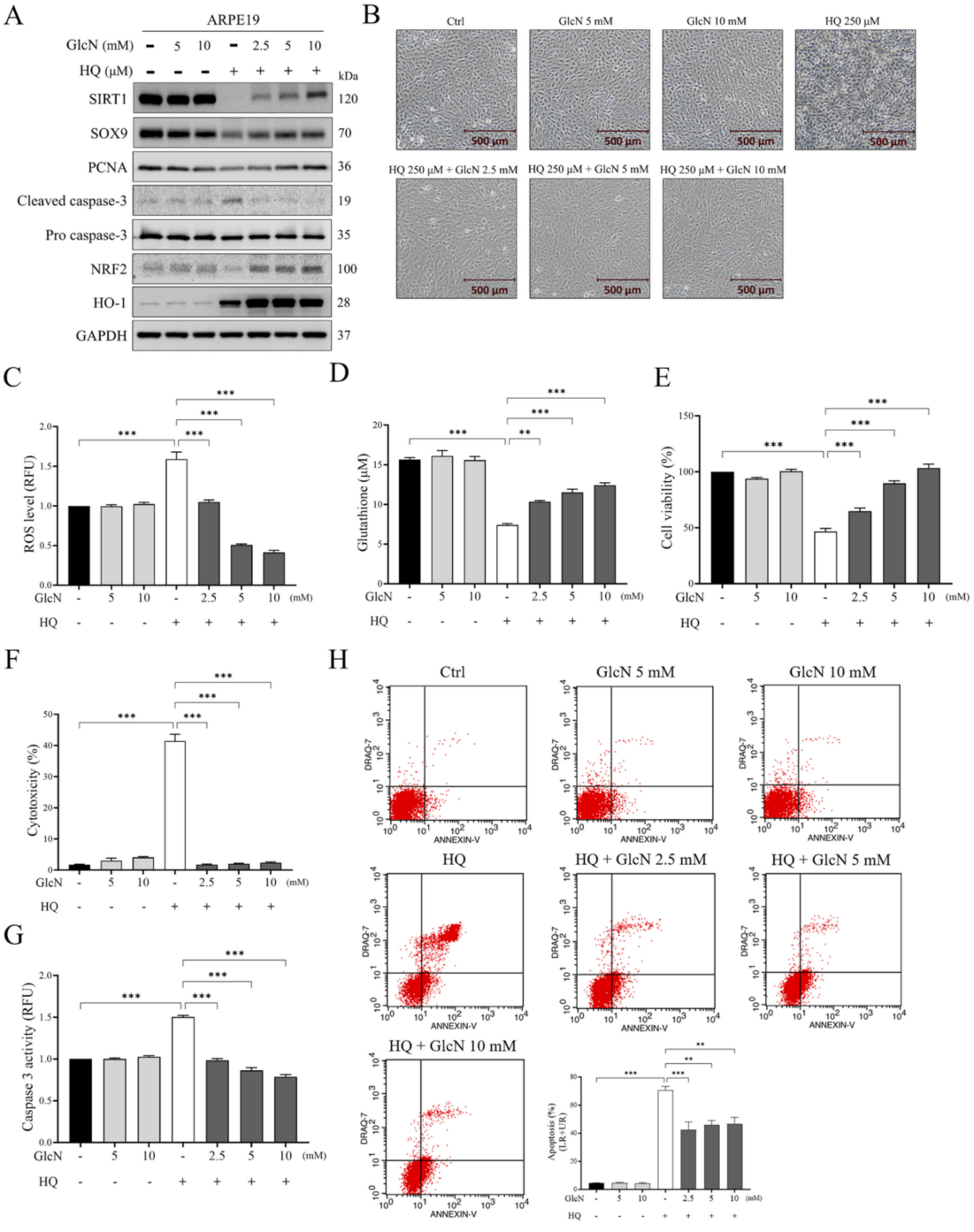


Figure 4. Glucosamine suppressed oxidative stress, SIRT1 downregulation, and cell damage in hydroquinone-exposed ARPE19 cells in a dose-dependent way. ARPE-19 cells were incubated with 250 μM of HQ in the presence or absence of various doses (2.5, 5, and 10 mM) of GlcN for 6 hours. (A) The expressions of SIRT1, SOX9, and markers of DNA repair (PCNA), apoptosis (cleaved caspase-3 and pro caspase-3), and oxidative stress (NRF2 and HO-1) were analyzed using Western blot analysis. (B) The morphological changes were examined and recorded using a microscopy equipped with a camera. (C) A ROS detection cell-based assay kit was applied to investigate intracellular reactive oxidative stress (ROS) levels. (D) The glutathione (GSH) levels were evaluated using a GSH assay kit. (E) The cell survival was detected using a cell counting kit-8 (CCK-8) reagent. (F) The cell cytotoxicity was determined using a lactate dehydrogenase (LDH) assay kit. (G) A caspase-3 assay kit was used to analyze the activity of caspase-3 activity in ARPE-19 cells after indicated treatments. (H) Apoptotic cells were stained with Annexin V-FITC and DRAQ7 and subsequently quantified using flow cytometry. Representative images are shown in upper panels and quantitative results of cell apoptosis are shown in lower panel. HQ, hydroquinone. GlcN, glucosamine. LR, lower right. UR, upper right. GAPDH was used as the loading control. **p < 0.01, ***p < 0.001 by one-way ANOVA followed by Bonferroni's post hoc test. Data are expressed as the mean ± SEM. SEM, error bars. Scale bar, 500 μm.

GlcN reversed HQ-induced pathology by restoring SIRT1 expression

We next explored whether GlcN could counteract HQ-induced RPE dysfunction by restoring SIRT1 levels. GlcN treatment increased the expressions of SIRT1, SOX9, PCNA, and NRF2 in HQ-treated cells and further elevated HO-1 expression (Figure 4A). In primary human RPE cells, the suppressive effect of HQ on the expressions of SIRT1 and SOX9 was also ameliorated by GlcN (Figure S2A). HQ-induced caspase-3 cleavage was significantly repressed by GlcN exposure (Figure 4A). The inhibitory effect of HQ on SIRT1 activity was ameliorated in cells exposed to GlcN (Figure S1B). In addition, GlcN reversed HQ-induced morphological changes (Figure 4B), ROS accumulation (Figure 4C), and glutathione depletion (Figure 4D). It also decreased cell damage (Figures 4E and 4F) and apoptosis, as indicated by reduced caspase-3 activity (Figure 4G) and Annexin V/DRAQ7-positive staining (Figure 4H) in HQ-exposed cells. The effect of GlcN in ameliorating HQ-induced ROS and apoptosis was also observed in primary RPE cells (Figure S2B and S2C). To determine whether GlcN's protective effect depended on SIRT1, we knocked down SIRT1 using siRNA. The expression of SIRT1 was significantly decreased in cells transfected with SIRT1 siRNA compared to those with scrambled siRNA (Figure 5A). Notably, SIRT1 inhibition diminished the effect of GlcN on the expressions of SIRT1, NRF2, HO-1, and cleaved caspase-3 in HQ-treated ARPE19 cells (Figure 5A). It also suppressed GlcN's ability to restore glutathione levels (Figure 5B), improve cell viability (Figure 5C), and reduce cell damage and apoptosis (Figures 5D-5F). These findings indicated that GlcN mitigated HQ-induced pathology via SIRT1 restoration.

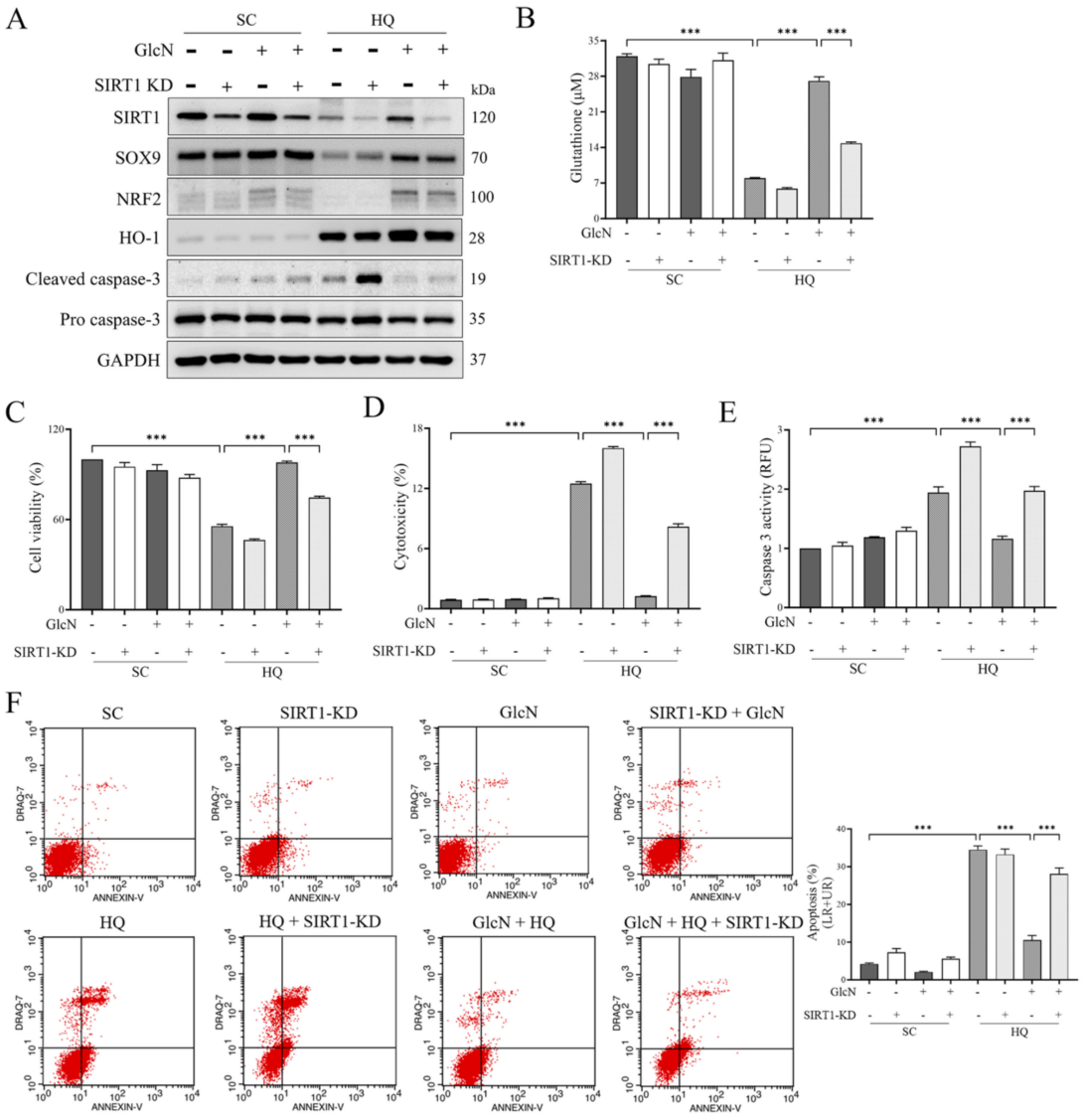


Figure 5. SIRT1 involved in the rescue effect of glucosamine on hydroquinone-induced cell damage and suppression of anti-oxidative machinery in ARPE-19 cells. ARPE-19 cells with/without SIRT1 silencing were treated with 250 μM of HQ and/or 10 mM of GlcN for 6 hours. (A) The expressions of SIRT1, SOX9, markers of

oxidative stress (NRF2 and HO-1) and apoptosis (cleaved caspase-3 and pro caspase-3) in ARPE-19 cells after indicated treatments were evaluated using Western blot analysis. (B) The amounts of glutathione (GSH) were detected using a GSH assay kit. (C) A cell counting kit-8 (CCK-8) reagent was used to investigate the cell survival of ARPE-19 cells after respective exposure. (D) The cell cytotoxicity was analyzed using a lactate dehydrogenase (LDH) assay kit. (E) The caspase-3 activity was measured using a caspase-3 assay kit. (F) Annexin V-FITC and DRAQ7-stained apoptotic cells were observed using flow cytometry. Representative images (left panels) and quantitative results (right panel) of apoptosis are shown. HQ, hydroquinone. SC, non-targeting siRNA-transfected cells. SIRT1-KD, SIRT1 siRNA-transfected cells. GAPDH served as the loading control. ***p < 0.001 by one-way ANOVA followed by Bonferroni's post hoc test. Data are expressed as the mean ± SEM. SEM, error bars.

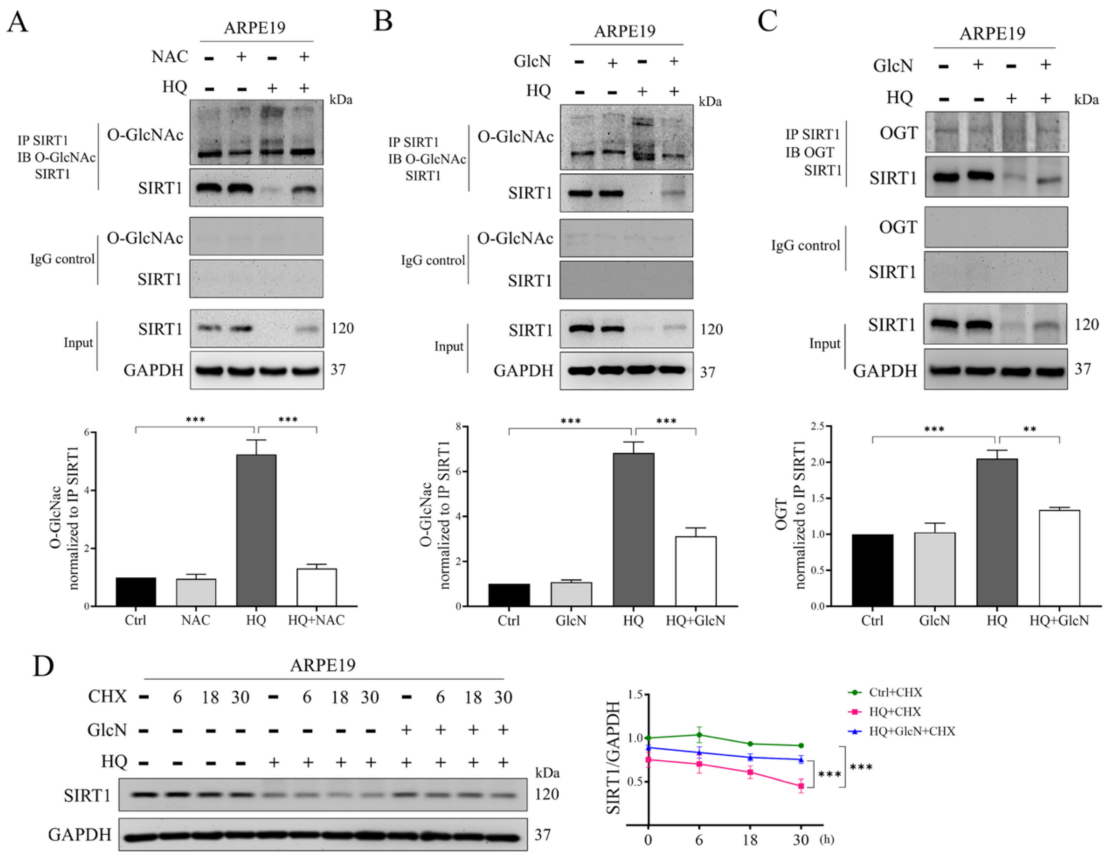


Figure 6. HQ exacerbated SIRT1 degradation through post-translationally increased glycosylation in ARPE-19 cells. Total lysates were extracted from ARPE-19 cells pre-treated with/without 5 mM of NAC (A) or 10 mM of GlcN (B and C) for 18 hours followed by exposure to 250 μM of HQ for 6 hours. (A and B) The glycosylation level of SIRT1 was evaluated using a co-immunoprecipitation (co-IP) assay. Western blot analysis of O-GlcNAc and SIRT1 in total extracts was performed after capturing with anti-SIRT1 or anti-mouse IgG antibodies and precipitating with protein G beads. (C) A co-IP assay was used to investigate the interaction between SIRT1 and OGT. Cell lysates were incubated with anti-SIRT1 or anti-mouse IgG antibodies, and the immune complexes were pulled down with protein G beads. The expressions of SIRT1 and OGT in precipitated lysates were evaluated using Western blot analysis. (D) ARPE-19 cells were pre-treated with/without 10 mM of GlcN for 18 hours and 250 μM of HQ for 4 hours followed by exposure to 50 μg/ml of translation inhibitor, CHX, for 6, 18, and 30 hours. After indicated treatments, the expression of SIRT1 in ARPE-19 cells was analyzed using Western blot analysis. HQ, hydroquinone. NAC, N-acetylcysteine. OGT, O-GlcNAc transferase. CHX, cycloheximide. GAPDH was used as the loading control. **p < 0.01, ***p < 0.001 by one-way ANOVA followed by Bonferroni's post hoc test or two-way ANOVA. Data are presented as the mean ± SEM. SEM, error bars.

GlcN ameliorated HQ-induced SIRT1 downregulation through decreasing interaction of SIRT1 with OGT and SIRT1 glycosylation

According to the results shown in Figure 3B, we noted that HQ did not alter mRNA expression of SIRT1, but it significantly reduced protein level of SIRT1 in ARPE-19 cells, suggesting a potential role of post-translational modification (PTM) on SIRT1 protein in HQ-modulated SIRT1 downregulation. PTM has been shown to be important in regulating protein activity, protein-protein interaction, and stability without changing mRNA level [33]. Previous studies have demonstrated elevated O-GlcNAcylation (glycosylation) on threonine and/or serine residues of SIRT1 was associated with increased enzymatic activity, cytoplasmic export, or ubiquitin-proteasome degradation of SIRT1 [34, 35]. Hence, we investigated whether SIRT1 glycosylation was involved in HQ-induced SIRT1 downregulation in ARPE-19 cells. Co-immunoprecipitation results revealed that HQ increased glycosylated SIRT1 level (Figures 6A and 6B), and that this effect was reversed by NAC (Figure 6A) and GlcN (Figure 6B). Given that O-GlcNAc transferase (OGT) catalyzes protein O-GlcNAcylation [36], we assessed its interaction with SIRT1. HQ enhanced the SIRT1-OGT interaction, and that this interaction was blocked in response to GlcN treatment (Figure 6C). To further validate the physical interaction between SIRT1 and OGT, we performed immunofluorescent staining in ARPE-19 cells. HQ exposure increased the spatial colocalization of SIRT1

and OGT, and that GlcN effectively reduced the HQ-induced colocalization of these two molecules (Figure S3A). Quantitative analysis of colocalization confirmed a significant elevation in the colocalization coefficient in response to HQ treatment, and this effect was markedly suppressed by GlcN exposure (Figure S3B). These results were consistent with co-IP findings, reinforcing that GlcN disrupted HQ-induced associations between SIRT1 and OGT. Using a cycloheximide (CHX) chase assay, we found HQ accelerated SIRT1 degradation, while GlcN stabilized the protein (Figure 6D). These findings indicated that HQ promotes SIRT1 instability via OGT-mediated glycosylation, a process that GlcN can counteract.

Discussion

In this study, we identified a novel pathological mechanism by which HQ, a major pro-oxidant component of cigarette smoke, induces RPE dysfunction. We demonstrated that HQ exposure led to a significant increase in intracellular ROS, inducing oxidative stress in RPE injury. We subsequently revealed that elevated ROS suppressed SIRT1 expression, suggesting that oxidative stress-driven downregulation of SIRT1 contributes to the observed cellular dysfunction. Both NAC and GlcN treatment restored SIRT1 levels and improved cellular resilience against HQ-induced injury. These findings confirmed a ROS-SIRT1 regulatory axis underlying HQ-mediated RPE damage and highlight the potential antioxidant strategies and SIRT1 modulators such as GlcN—in AMD (Figure 7).

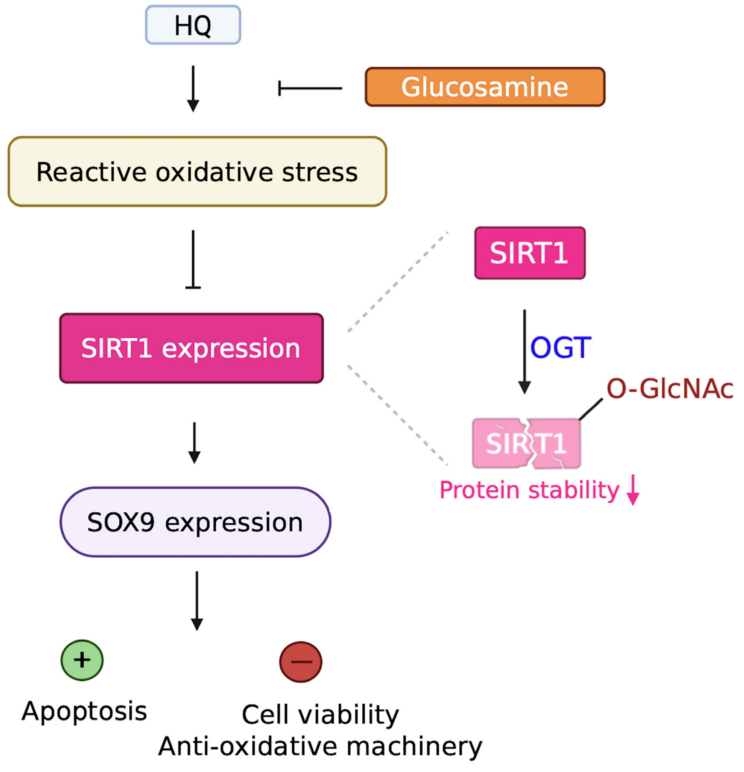


Figure 7. HQ induced dysfunction of ARPE-19 cells through decreasing stability of glycosylated SIRT1. HQ caused AMD-related conditions in ARPE-19 cells through decreasing expressions of SIRT1 and SOX9, and that ROS acted as an upstream regulator in mediating downregulation of these molecules. Mechanistically, HQ promoted interaction between OGT and SIRT1, thereby increasing glycosylation of SIRT1 and decreasing its stability. In addition, GlcN ameliorated cell damage of HQ-exposed ARPE-19 cells through reversing glycosylation and degradation of SIRT1.

Cigarette smoking is a well-established modifiable risk factor for AMD [7], with a two- to four-fold increased risk of late-stage AMD among smokers compared to non-smokers [37]. Mechanistically, this association has been largely attributed to cigarette smoke-induced oxidative stress, chronic inflammation, and pathological angiogenesis [38, 39]. HQ, a toxic quinone component of cigarette smoke, has been known to disrupt mitochondrial function, elevate ROS levels, and induce apoptosis in RPE cells [16, 18]. Our study confirmed that HQ exposure results in elevated ROS production, depletion of antioxidant defenses, and increased apoptosis in ARPE-19 cells. However, some discrepancies remain across the literature. For instance, while HQ-induced oxidative stress has been widely observed, low-dose HQ exposure has been reported to trigger transient antioxidant responses, potentially providing short-term cellular protection [40]. These variations likely reflect differences in genetic background, cellular adaptive mechanisms, or compensatory pathways that influence the cellular response to cigarette smoke constituents.

SIRT1 is regulated at multiple levels—transcriptional, post-transcriptional, translational, and post-translational. Among PTMs, O-GlcNAcylation has emerged as a key regulator of SIRT1 stability, enzymatic activity, and localization [34, 35]. Our findings revealed that HQ promotes SIRT1 degradation through enhanced O-GlcNAcylation, leading to its destabilization in ARPE-19 cells. This observation aligns with previous reports suggesting that excessive O-GlcNAcylation impairs SIRT1 function and promotes its proteasomal degradation [35]. Nonetheless, other studies have reported that under metabolic stress, O-GlcNAcylation enhances SIRT1 activity and promotes its cytoplasmic localization [34, 35]. These conflicting observations suggest that the effects of O-GlcNAcylation on SIRT1 are context-dependent and modulated by the cellular environment, glycosylation extent, and crosstalk with other PTMs like phosphorylation or

acetylation. While earlier work by Han et al. suggested that O-GlcNAcylation enhances SIRT1 activity, and Chattopadhyay et al. identified O-GlcNAcylation-mediated SIRT1 degradation as a physiological switch during hepatic refeeding [34, 35], our study provides a distinct pathogenic perspective. We demonstrated that under environmental stress, such as cigarette smoke-derived HQ, excessive O-GlcNAcylation acts as a primary signal for SIRT1 destabilization and functional impairment, rather than a homeostatic metabolic response. Crucially, we identified that both NAC and GlcN effectively reverse HQ-induced SIRT1 glycosylation and preserve protein stability, highlighting targetable PTM nodes for mitigating oxidant-induced RPE cellular dysfunction. These results suggest potential therapeutic strategies for mitigating cigarette smoke-induced RPE dysfunction and AMD progression through modulation of SIRT1 PTMs.

SIRT1 has been implicated in pathways related to AMD, acting as both a protector and a contributor to disease progression. While many studies have supported SIRT1's role in attenuating oxidative stress and inflammation [41], others have suggested that excessive SIRT1 activation may exacerbate pathological angiogenesis or metabolic imbalance [42]. These conflicting roles likely stem from variations in AMD subtypes, experimental models, and differential downstream target regulation. One such downstream effector is SOX9, a transcription factor essential for retinal development and RPE homeostasis [43]. Our results showed that HQ-induced downregulation of SIRT1 led to a reduction in SOX9 expression, contributing to RPE dysfunction. SIRT1 has been revealed to deacetylate SOX9, facilitate its nuclear translocation and increase its transcriptional activity [44]. Sox9, a transcription factor, has been demonstrated to regulate the expressions of visual cycle genes, and that conditional inactivation of *Sox9* in mouse RPE remarkably decreases the expressions of visual cycle genes, including *Rpe65, Rgr, Lrat, Rlbp1, Rdh5,* and *Rbp1*, and cause RPE degeneration [45]. These results suggested the involvement of SOX9 in maintaining retinal homeostasis. Apart from SOX9, several downstream molecules of SIRT1, including FOXO3a, p53, and peroxisome proliferator-activated receptor-γ coactivator 1α (PGC-1α) have been implicated in mediating age-related ocular diseases. FOXO3a has been noted to modulate aging process, including cell cycle arrest, apoptosis, autophagy, oxidative stress, and DNA repair, and that activation of FOXO3a-associated antioxidant pathway has been shown to protect RPE from oxidative stress [46]. Moreover, PGC1α, which functions as a master regulator of mitochondrial biogenesis and oxidative metabolism, has been shown to be highly expressed in healthy retina and regulate autophagy and antioxidant defense of RPE [47]. On the other hand, age-related activation of p53 has been revealed to stimulate apoptosis of RPE cells through elevated expressions of PUMA (p53 upregulated modulator of apoptosis) and active caspase-3 [48].

Our study showed that GlcN restored SIRT1 protein levels in HQ-exposed ARPE-19 cells, suggesting a protective role against oxidative damage and RPE degeneration. In chondrocytes, GlcN also increases SIRT1 expression and promotes type II collagen (COL2A1) expression, conferring protective effects in osteoarthritis [30]. Conversely, studies have reported that GlcN reduces SIRT1 levels under certain conditions. In pancreatic β-cells, GlcN stimulation of the hexosamine biosynthesis pathway (HBP) has been shown to lower SIRT1 expression and induce apoptosis [49]. In addition, reduced SIRT1 expression has been observed in GlcN-induced insulin-resistant HepG2 cells [50]. These contradictory findings suggest that in the RPE and chondrocytes, GlcN favors the stabilization or transcriptional induction of SIRT1 over the degradative and suppressive pathways observed in glucotoxic or insulin-resistant metabolic conditions. Hence, the effects of GlcN on SIRT1 are highly context-dependent and are determined by both the cell types and the nature of the pathological stimulus.

Our results revealed that HQ increased HO-1 expression, whereas GlcN treatment and SIRT1 overexpression further enhanced HO-1 protein levels in HQ-exposed cells (Figures 3C and 4A). HO-1 has been characterized by its dual roles in cellular physiology, acting as both a cytoprotective regulator and a potential mediator of cellular injury depending on the magnitude and duration of its induction [51]. Moderate HO-1 induction generally functions as an adaptive antioxidant response, whereas excessive or sustained activation may promote iron-dependent oxidative injury and ferroptosis [52]. While excessive HO-1 activity has been shown to drive iron-mediated damage, our functional data demonstrated a reduction in ROS levels and an increase in GSH levels in HQ-treated cells after GlcN exposure (Figure 4C and 4D), suggesting that HO-1 induction remained predominantly cytoprotective rather than the cause of oxidative damage under our experimental conditions. Furthermore, GlcN and ectopic expression of SIRT1 remarkably decreased HQ-induced LDH release and cell apoptosis in ARPE-19 cells (Figure 3H, 3J, 4F, and 4H). These findings indicated that upregulation of HO-1 in response to GlcN treatment or SIRT1 overexpression in HQ-exposed cells represented a regulated adaptive response rather than a pathological signal. Collectively, the GlcN/SIRT1-mediated

induction of HO-1 appears to remain within a cytoprotective range, contributing to the restoration of redox homeostasis without evidence of the iron-dependent oxidative injury associated with excessive HO-1 activation.

While our findings demonstrated a clear molecular mechanism for HQ-induced SIRT1 degradation in primary and cultured RPE cells, the lack of *in vivo* validation remains a critical limitation, and further animal studies are warranted to confirm the physiological significance and therapeutic potential of these pathways.

In conclusion, this study identified the ROS-OGT-SIRT1 axis as a critical signaling cascade in mediating HQ-induced oxidative stress and injury in RPE cells. HQ elevated ROS levels, leading to SIRT1 downregulation via enhanced OGT-SIRT1 interaction and increased O-GlcNAcylation. Antioxidant NAC confirmed the upstream regulatory role of ROS, while GlcN effectively stabilized SIRT1 expression and mitigated cellular damage. These findings highlight SIRT1 as a key regulator of RPE cellular homeostasis under HQ-induced oxidative stress and support further *in vivo* studies to validate this pathway in RPE pathogenesis.

Supplementary Material

Supplementary figures and tables.
https://www.medsci.org/v23p3754s1.pdf

Acknowledgements

Funding

This work was supported by Tri-Service General Hospital, Taiwan, Republic of China (TSGH-D-114123, TSGH-E-114266); Ministry of National Defense, Taiwan, Republic of China (MND-MAB-D-114117); and C. Y. Chai Foundation for the Advancement of Education, Sciences, and Medicine. All the funders had no role in study design, data collection and analysis, decision to publish, or preparation of the manuscript.

Data availability

Data will be made available on request.

Competing Interests

The authors have declared that no competing interest exists.

References

1. Zhang Z, Liang F, Chang J, Shan X, Yin Z, Wang L, et al. Autophagy in dry AMD: A promising therapeutic strategy for retinal pigment epithelial cell damage. Exp Eye Res. 2024; 242: 109889.
2. Marchesi N, Capierri M, Pascale A, Barbieri A. Different Therapeutic Approaches for Dry and Wet AMD. Int J of Mol Sci; 2024. p. 13053.
3. Domalpally A, Danis RP, Trane R, Blodi BA, Clemons TE, Chew EY. Atrophy in Neovascular Age-Related Macular Degeneration: Age-Related Eye Disease Study 2 Report Number 15. Ophthalmol Retina. 2018; 2: 1021-7.
4. Mimura T, Noma H. Title Oxidative Stress in Age-Related Macular Degeneration: From Molecular Mechanisms to Emerging Therapeutic Targets. Antioxidants; 2025. p. 1251.
5. Ferrington DA, Ebeling MC, Kapphahn RJ, Terluk MR, Fisher CR, Polanco JR, et al. Altered bioenergetics and enhanced resistance to oxidative stress in human retinal pigment epithelial cells from donors with age-related macular degeneration. Redox Biol. 2017; 13: 255-65.
6. Mitchell P, Liew G, Gopinath B, Wong TY. Age-related macular degeneration. Lancet (London, England). 2018; 392: 1147-59.
7. Smith W, Assink J, Klein R, Mitchell P, Klaver CC, Klein BE, et al. Risk factors for age-related macular degeneration: Pooled findings from three continents. Ophthalmology. 2001; 108: 697-704.
8. Mitchell P, Wang JJ, Smith W, Leeder SR. Smoking and the 5-year incidence of age-related maculopathy: the Blue Mountains Eye Study. Arch Ophthalmol. 2002; 120: 1357-63.
9. Detaram HD, Joachim N, Liew G, Vu KV, Burlutsky G, Mitchell P, et al. Smoking and treatment outcomes of neovascular age-related macular degeneration over 12 months. Br J Ophthalmol. 2020; 104: 893-8.
10. Khudhur ZO, Smail SW, Awla HK, Ahmed GB, Khdhir YO, Amin K, et al. The effects of heavy smoking on oxidative stress, inflammatory biomarkers, vascular dysfunction, and hematological indices. Sci Rep. 2025; 15: 18251.
11. Das TN, Dey S, Chowdhury IJ, Hossen JM, Nishat RJ, Chowdhury R, et al. Evaluation of Plasma Fibrinogen Level, Platelet Count & Lipid Profile as Predictors of Cardiovascular Disease among Bangladeshi Healthy Male Smokers. Asian J Med Health. 2024; 22: 182-93.
12. Bertram KM, Baglole CJ, Phipps RP, Libby RT. Molecular regulation of cigarette smoke induced-oxidative stress in human retinal pigment epithelial cells: implications for age-related macular degeneration. Am J Physiol Cell Physiol. 2009; 297: C1200-10.
13. Zhu Q, Liu M, He Y, Yang B. Quercetin protect cigarette smoke extracts induced inflammation and apoptosis in RPE cells. Artif Cell Nanomed Biotechnol. 2019; 47: 2010-5.
14. Espinosa-Heidmann DG, Suner IJ, Catanuto P, Hernandez EP, Marin-Castano ME, Cousins SW. Cigarette smoke-related oxidants and the development of sub-RPE deposits in an experimental animal model of dry AMD. IOVS. 2006; 47: 729-37.
15. Hess R, Brahmajothi MV, Saloupis P, Mettu PS, Cousins SW. Repetitive periocular injection of hydroquinone promotes mitochondrial dysfunction in retinal pigment epithelium of mouse eyes. IOVS. 2015; 56: 1277-.
16. Sharma A, Patil JA, Gramajo AL, Seigel GM, Kuppermann BD, Kenney CM. Effects of hydroquinone on retinal and vascular cells *in vitro*. Indian J Ophthalmol. 2012; 60: 189-93.
17. Abokyi S, Shan SW, Lam CH, Catral KP, Pan F, Chan HH, et al. Targeting Lysosomes to Reverse Hydroquinone-Induced Autophagy Defects and Oxidative Damage in Human Retinal Pigment Epithelial Cells. Int J Mol Sci. 2021; 22.
18. Bhattarai N, Korhonen E, Mysore Y, Kaarniranta K, Kauppinen A. Hydroquinone Induces NLRP3-Independent IL-18 Release from ARPE-19 Cells. Cells. 2021; 10.
19. Neal SE, Buehne KL, Besley NA, Yang P, Silinski P, Hong J, et al. Resveratrol Protects Against Hydroquinone-Induced Oxidative Threat in Retinal Pigment Epithelial Cells. IOVS. 2020; 61: 32-.
20. Wu Q-J, Zhang T-N, Chen H-H, Yu X-F, Lv J-L, Liu Y-Y, et al. The sirtuin family in health and disease. Signal Transduct Target Ther. 2022; 7: 402.
21. Sun H, Li D, Wei C, Liu L, Xin Z, Gao H, et al. The relationship between SIRT1 and inflammation: a systematic review and meta-analysis. Front Immunol. 2024; 15: 1465849.
22. Zhang M, Jiang N, Chu Y, Postnikova O, Varghese R, Horvath A, et al. Dysregulated metabolic pathways in age-related macular degeneration. Sci Rep. 2020; 10: 2464.
23. Chen Y, Chen J, Yun L, Xu L, Liu J, Xu Y, et al. Hydroquinone-induced malignant transformation of TK6 cells by facilitating SIRT1-mediated p53 degradation and up-regulating KRAS. Toxicol Lett. 2016; 259: 133-42.
24. Chang C, Ibi A, Zhang Y, Du M, Roh YS, O'Brien R, et al. Does Salt Form Matter? A Pilot Randomized, Double-Blind, Crossover Pharmacokinetic Comparison of Crystalline and Regular Glucosamine Sulfate in Healthy Volunteers. Nutrients; 2025. p. 2491.
25. Feng KM, Chien WC, Chen JT, Chen YH, Chung CH, Sun CA, et al. The impact of glucosamine on age-related macular degeneration in patients: A nationwide, population-based cohort study. PloS one. 2021; 16: e0251925.
26. Chen JT, Liang JB, Chou CL, Chien MW, Shyu RC, Chou PI, et al. Glucosamine sulfate inhibits TNF-alpha and IFN-gamma-induced production of ICAM-1 in human retinal pigment epithelial cells *in vitro*. IOVS. 2006; 47: 664-72.
27. Chen CL, Liang CM, Chen YH, Tai MC, Lu DW, Chen JT. Glucosamine modulates TNF-α-induced ICAM-1 expression and function through O-linked and N-linked glycosylation in human retinal pigment epithelial cells. IOVS. 2012; 53: 2281-91.
28. Chen YJ, Huang YS, Chen JT, Chen YH, Tai MC, Chen CL, et al. Protective effects of glucosamine on oxidative-stress and ischemia/reperfusion-induced retinal injury. IOVS. 2015; 56: 1506-16.
29. Chen CL, Chen YH, Liang CM, Tai MC, Lu DW, Chen JT. Glucosamine-Induced Autophagy through AMPK¯mTOR Pathway Attenuates Lipofuscin-

Like Autofluorescence in Human Retinal Pigment Epithelial Cells *In Vitro*. Int J Mol Sci. 2018; 19.
30. Igarashi M, Sakamoto K, Nagaoka I. Effect of glucosamine on expression of type II collagen, matrix metalloproteinase and sirtuin genes in a human chondrocyte cell line. Int J Mol Med. 2017; 39: 472-8.
31. Zheng J, Zhao L, Liu Y, Chen M, Guo X, Wang J. N-acetylcysteine, a small molecule scavenger of reactive oxygen species, alleviates cardiomyocyte damage by regulating OPA1-mediated mitochondrial quality control and apoptosis in response to oxidative stress. J Thorac Dis. 2024; 16: 5323-36.
32. He M, Long P, Yan W, Chen T, Guo L, Zhang Z, et al. ALDH2 attenuates early-stage STZ-induced aged diabetic rats retinas damage via Sirt1/Nrf2 pathway. Life Sci. 2018; 215: 227-35.
33. Suskiewicz MJ. The logic of protein post-translational modifications (PTMs): Chemistry, mechanisms and evolution of protein regulation through covalent attachments. Bioessays. 2024; 46: e2300178.
34. Han C, Gu Y, Shan H, Mi W, Sun J, Shi M, et al. O-GlcNAcylation of SIRT1 enhances its deacetylase activity and promotes cytoprotection under stress. Nat Commun. 2017; 8: 1491.
35. Chattopadhyay T, Maniyadath B, Bagul HP, Chakraborty A, Shukla N, Budnar S, et al. Spatiotemporal gating of SIRT1 functions by O-GlcNAcylation is essential for liver metabolic switching and prevents hyperglycemia. PNAS. 2020; 117: 6890-900.
36. Wulff-Fuentes E, Berendt RR, Massman L, Danner L, Malard F, Vora J, et al. The human O-GlcNAcome database and meta-analysis. Sci Data. 2021; 8: 25.
37. Heesterbeek TJ, Lorés-Motta L, Hoyng CB, Lechanteur YTE, den Hollander AI. Risk factors for progression of age-related macular degeneration. Ophthalmic Physiol Opt. 2020; 40: 140-70.
38. Lambert NG, ElShelmani H, Singh MK, Mansergh FC, Wride MA, Padilla M, et al. Risk factors and biomarkers of age-related macular degeneration. Prog Retin Eye Res. 2016; 54: 64-102.
39. Seddon JM, George S, Rosner B. Cigarette smoking, fish consumption, omega-3 fatty acid intake, and associations with age-related macular degeneration: the US Twin Study of Age-Related Macular Degeneration. Arch Ophthalmol. 2006; 124: 995-1001.
40. Cho JY. Suppressive effect of hydroquinone, a benzene metabolite, on *in vitro* inflammatory responses mediated by macrophages, monocytes, and lymphocytes. Mediat Inflamm. 2008; 2008: 298010.
41. Meng T, Qin W, Liu B. SIRT1 Antagonizes Oxidative Stress in Diabetic Vascular Complication. Front Endocrinol. 2020; 11: 568861.
42. Kauppinen A, Paterno JJ, Blasiak J, Salminen A, Kaarniranta K. Inflammation and its role in age-related macular degeneration. Cell Mol Life Sci. 2016; 73: 1765-86.
43. Hurtado A, López-Soriano V, Lao M, Celis-Barroso MA, Lazúen P, Chacón-de-Castro A, et al. Sox9 prevents retinal degeneration and is required for limbal stem cell differentiation in the adult mouse eye. Elife. 2025; 13.
44. Ming Z, Vining B, Bagheri-Fam S, Harley V. SOX9 in organogenesis: shared and unique transcriptional functions. CMLS. 2022; 79: 522.
45. Masuda T, Wahlin K, Wan J, Hu J, Maruotti J, Yang X, et al. Transcription factor SOX9 plays a key role in the regulation of visual cycle gene expression in the retinal pigment epithelium. J Biol Chem. 2014; 289: 12908-21.
46. Hao XD, Liu JX, Zhang JS. Longevity factor FOXO3a: A potential therapeutic target for age-related ocular diseases. Life Sci. 2024; 350: 122769.
47. Zhang M, Chu Y, Mowery J, Konkel B, Galli S, Theos AC, et al. Pgc-1α repression and high-fat diet induce age-related macular degeneration-like phenotypes in mice. DMM. 2018; 11.
48. Bhattacharya S, Chaum E, Johnson DA, Johnson LR. Age-related susceptibility to apoptosis in human retinal pigment epithelial cells is triggered by disruption of p53-Mdm2 association. IOVS. 2012; 53: 8350-66.
49. Lafontaine-Lacasse M, Doré G, Picard F. Hexosamines stimulate apoptosis by altering SIRT1 action and levels in rodent pancreatic β-cells. J Endocrinol. 2011; 208: 41-9.
50. Sun C, Zhang F, Ge X, Yan T, Chen X, Shi X, et al. SIRT1 improves insulin sensitivity under insulin-resistant conditions by repressing PTP1B. Cell Metab. 2007; 6: 307-19.
51. Chiang SK, Chen SE, Chang LC. The Role of HO-1 and Its Crosstalk with Oxidative Stress in Cancer Cell Survival. Cells. 2021; 10.
52. Ma Y, Zhang D, Li Z. Dual role of Heme oxygenase-1 in disease progression and treatment: A literature review. Int J Biol Macromol. 2025; 321: 146272.